Local piezoresponse and polarization switching in nucleobase thymine microcrystals

Igor Bdikin' , Alejandro Heredia, Sabine M. Neumayer, Vladimir S. Bystrov' , José Gracio' , Brian J. Rodriguez, and Andrei L. Kholkin'

Citation: Journal of Applied Physics **118**, 072007 (2015); doi: 10.1063/1.4927806
View online: http://dx.doi.org/10.1063/1.4927806
View Table of Contents: http://aip.scitation.org/toc/jap/118/7
Published by the American Institute of Physics

Local piezoresponse and polarization switching in nucleobase thymine microcrystals

Igor Bdikin,[1,a)] Alejandro Heredia,[2] Sabine M. Neumayer,[3,4] Vladimir S. Bystrov,[5,b)] José Gracio,[1,c)] Brian J. Rodriguez,[3,4] and Andrei L. Kholkin[5,d)]
[1]*Department of Mechanical Engineering, Centre for Mechanical Technology and Automation, University of Aveiro, 3810 193 Aveiro, Portugal*
[2]*Departamento de Química de Radiaciones y Radioquímica, Instituto de Ciencias Nucleares, Universidad Nacional Autónoma de México, Circuito Exterior C.U. Apdo. Postal 70 543, 04510 México, D.F., Mexico*
[3]*School of Physics, University College Dublin, Belfield, Dublin 4, Ireland*
[4]*Conway Institute of Biomolecular and Biomedical Research, University College Dublin, Belfield, Dublin 4, Ireland*
[5]*Department of Physics and CICECO Aveiro Institute of Materials, University of Aveiro, 3810 193 Aveiro, Portugal*

(Received 25 October 2014; accepted 24 February 2015; published online 19 August 2015)

Thymine (2-oxy-4-oxy-5 methyl pyrimidine) is one of the four nucleobases of deoxyribonucleic acid (DNA). In the DNA molecule, thymine binds to adenine via two hydrogen bonds, thus stabilizing the nucleic acid structure and is involved in pairing and replication. Here, we show that synthetic thymine microcrystals grown from the solution exhibit local piezoelectricity and apparent ferroelectricity, as evidenced by nanoscale electromechanical measurements via Piezoresponse Force Microscopy. Our experimental results demonstrate significant electromechanical activity and polarization switchability of thymine, thus opening a pathway for piezoelectric and ferroelectric-based applications of thymine and, perhaps, of other DNA nucleobase materials. The results are supported by molecular modeling of polarization switching under an external electric field. © *2015 AIP Publishing LLC*. [http://dx.doi.org/10.1063/1.4927806]

INTRODUCTION

Thymine ($C_5H_6N_2O_2$, 2-oxy-4-oxy-5 methyl pyrimidine) is one of the four bases of deoxyribonucleic acid (DNA), which plays a fundamental role in the storage and transfer of genetic information. Thymine, along with adenine, guanine, and cytosine are the building blocks of DNA, and understanding their structure at the molecular level allows for better apprehension of their function and generic features. For example, a common mutation of DNA involves two adjacent thymines or cytosines, which, when illuminated with the UV light, may form pyrimidine dimers causing "kinks" in the DNA molecular structure that inhibit normal replication.[1] This kind of mutation can cause a life-threatening melanoma with evolutionary implications and prebiotic importance for molecular complexation. Furthermore, much effort has been spent on studying hydrogen bonding in intermolecular interactions in nucleobases because hydrogen bonds between DNA molecules play a decisive role in the stabilization and thus transfer of biological information.[2–4] Moreover, DNA is more stable than RNA (ribonucleic acid), and thymine is in DNA not RNA, so it can be said that thymine is involved in the longer information storage ability in DNA.

In the past, the research on nucleobase materials has been mostly focused on the study of nucleobase molecules, while the study of synthetic crystals (including thymine) has received much less attention.[5–7] These studies can be helpful not only for understanding the role of hydrogen bonds in the formation of self-assembled or organized structures, but also for the practical applications in microelectronics and micromechanics.[8–14] For example, the unique electronic properties of deoxyribonucleic acid have allowed DNA to be used as an electron blocking layer in organic light-emitting devices (OLED) and organic photovoltaic cells and as gates in thin-film transistors.[15] Extensive debates regarding charge transport in DNA, which is basically due to the overlap of delocalized π states, are ongoing.[16,17] From the electronic point of view, thymine is a wide band-gap semiconductor, with the forbidden band gap of about 4 eV, and its electronic structure at the surface can be modified by using a specific metal to form a contact barrier.[18,19] Another aspect of the thymine molecule is its large intrinsic dipole moment (about 4 Debyes)[20] that may give rise to useful electromechanical effects (such as piezoelectricity) due to electric field-induced conformation in a material. As such, possible piezoelectricity in thymine can be a base of future miniaturized biosensors intrinsically compatible with the DNA molecule[21] or be a part of complex micro- and nanomechanical systems useful, for example, for DNA sequencing.[22]

In recent years, the use of highly sensitive Piezoresponse Force Microscopy (PFM) enabled nanoscale electromechanical

[a)]Author to whom correspondence should be addressed. Electronic mail: bdikin@ua.pt
[b)]Also with Institute of Mathematical Problems of Biology, Puschino, Moscow District, Russia.
[c)]Deceased 11 October 2014.
[d)]Also with Institute of Natural Sciences, Ural Federal University, Ekaterinburg 620000, Russia.

characterization of various biomaterials including elastin,[23] teeth,[24] cartilage,[25] diphenylalanine nanotubes,[26] amino acids,[27] hydroxyapatite,[28] and other polar materials including a large number of ferroelectric perovskites.[29,30] In this work, we report on sufficiently strong piezoelectricity and switchable polarization in thymine microcrystals grown from the solution. This observation may open up various possibilities of using crystalline thymine in microelectromechanical systems, in nanobiotechnology and as switching elements in microelectronic applications.

EXPERIMENTAL METHODS

Sample preparation

Thymine (Sigma-Aldrich CAS 65-71-4) crystals were grown by slow evaporation of water solutions with different thymine concentrations (0.1 1.0 mg ml ^{1}) in ultra pure deionized water. Approximately 0.5 ml of the aqueous solution was dropped onto a Pt coated SiO_2/(100)Si substrate and left for crystallization at room temperature under ambient conditions.

X-ray diffraction

The powder X-ray diffraction (XRD) patterns of thymine microcrystals were collected at room temperature in a continuous scanning mode (step 0.02° and time 10 s) on a Siemens D500 diffractometer with a secondary monochromator CuKα X-radiation in the range $2\theta = 5°$ 60°.

Electromechanical and ferroelectric characterization

Thymine microcrystals were simultaneously visualized by using contact mode AFM and PFM methods. The PFM technique is based on the detection of the mechanical response of the sample to an applied electric voltage due to converse piezoelectric effect. A conductive Si cantilever (Nanosensors, nominal force constant 15 N/m) was used to both apply the voltage to the surface and to measure the mechanical response of the sample. In our study, a commercial AFM (Ntegra Prima, NT-MDT) was equipped with an external lock-in amplifier (SR-830, Stanford Research) and a function generator (FG-120, Yokogawa), which were used in order to apply both ac and dc voltages to the surface of the crystals for poling and piezoresponse image acquisition.[27] The voltage applied to the tip is a sine wave ($U_{ac}\sin(\omega t)$). Under this voltage the piezoresponse signal $\Delta z(\omega) = d_{33eff} V_{ac}(\omega)$ is detected by the photodiode due to sample deformation. The amplitude $A(\varpi)$ and phase difference $\Phi(\varpi)$ of this vibration are measured with a lock-in amplifier. Domains with different polarization orientations obtained by PFM are distinguished by piezoresponse amplitude $A(\varpi) \sim \Delta z(V_{ac})$ dependent on the value and orientation of polarization and by phase $\Phi(\varpi)$ which is about 0 and 180° for domains with opposite polarization orientation. In this way, mapping of $A(\varpi)\cos(\Phi(\varpi))$ allows to get full information on the local polarization distribution.

To prove the presence of ferroelectric polarization, we performed PFM switching analysis to obtain local piezoresponse hysteresis loops in which the polarization state is changed by the application of a sequence of poling pulses.[31] In the poling experiments, the tip was fixed at a predefined position on the surface and external bias pulse was applied. After poling, this area was scanned again and the polarization was probed using PFM imaging.

Molecular modeling

To gain insight into the molecular-scale ferroelectric switching of thymine and to calculate the values of spontaneous polarization and corresponding piezoelectric moduli, molecular modeling using HyperChem 8.0 software was performed, similar to Refs. 32 36. The quantum-chemical PM3 method with both restricted (RHF) and unrestricted Hartree-Fock (UHF) approximations was used. Crystal structure was explored by local density approximation (LDA) of density functional theory (DFT) with first-principle calculations on the base of AIMPRO code.[32,33,35] The basis set for each of the used atoms was taken from the AIMPRO library.[32] We used single point (SP) calculations as well geometrical optimization (total energy optimization). Using constructed unit cell from previous AIMPRO calculations, we transform all coordinates to Cartesian ones by standard OpenBabel program and then work with molecular model of thymine structures using HyperChem 8.0 program.[35] External electric field was introduced using a special option in HyperChem, which allowed us to simulate the polarization switching in both SP and optimization regimes. Such an approach gave us a possibility to control the displacements of all atoms to new equilibrium positions and corresponding dipole moment and polarization. The data in Table II were obtained as a difference between the zero field and in-field positions of the atoms. As for the electrostriction coefficient, it was derived by calculating the volume change of the elementary cell under applied electric field.

RESULTS AND DISCUSSION

The obtained XRD patterns (shown in Fig. 1) substantiate the presence of both thymine anhydrate and thymine monohydrate phases in the as-grown microcrystals. The positions of the thymine anhydrate peaks were found to be in a close agreement with the data available from the Joint Committee on Powder Diffraction Standards (JCPDS) file (No. 00-039-1576). The fitting of XRD peaks confirmed that the thymine anhydrate crystal structure is compatible with a monoclinic group with the following unit cell parameters: a = 12.700 Å, b = 6.816 Å, c = 6.725 Å, and $\beta = 105.23°$. However, some minor peaks were found in the XRD patterns that were attributed to the presence of thymine monohydrate phase (Fig. 1(a)). As expected, the volume fraction of thymine monohydrate significantly increased with decreasing thymine concentration in the solution (see the XRD results for 0.1 mg·ml ^{1} concentration in Fig. 1(b) and comparison of 1.0 and 0.1 mg·ml ^{1} concentrations in the inset). Intensities of XRD peaks are not in agreement with the JCPDS data. We explain the reduced number of peaks on XRD by the texture effect of microcrystals due to their orientations on the substrates. h00 is a predominant peak for thymine anhydrate and 0k0 is for thymine monohydrate. As it is known from the literature, the space group for both thymine anhydrate and monohydrate

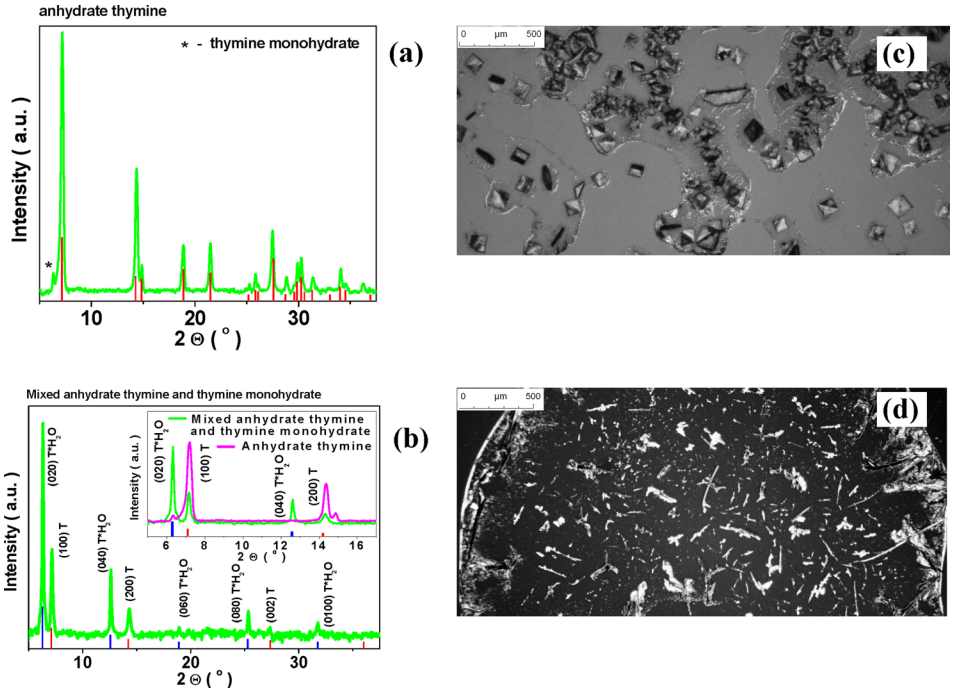

FIG. 1. (a) X ray diffraction pattern of the thymine crystals grown from 1.0 mg ml ^{1} (a) and 0.1 mg ml ^{1} (b) thymine solution (green), the corresponding Bragg positions of thymine anhydrate (red) and thymine monohydrate (blue). (c) Representative optical image (from 1.0 mg ml ^{1} thymine solution) of thymine crystals. (d) Representative optical image (from 0.1 mg ml ^{1} thymine solution) of thymine crystals. The inset to (b) shows X ray diffraction pattern in the small interval of the pure thymine and mixed thymine anhydrate and thymine monohydrate.

crystals[37,38] is centrosymmetric ($P2_1/c$) in which piezoelectricity is not permitted. Therefore, no piezoelectric activity was found in large thymine anhydrate crystals by PFM measurements. However, large dipole moment of the thymine molecule[20] may readily induce polar distortions in the grown *microcrystals*. The lattice parameter *b* for thymine monohydrate for our microcrystals was found to be 28.150 Å (Fig. 1(b)), i.e., different from the parameter *b* reported for thymine powder[38] (27.862 Å). We hypothesize that significant structural distortions due to the presence of water in the crystal lattice might be an indication of the potential polar behavior[39–41] as will be experimentally delineated below.

Figures 1(c) and 1(d) show the representative optical images of the investigated thymine crystals grown on Pt/SiO_2/Si substrates with two different thymine concentrations (0.1 and 1.0 mg ml ^{1}) of the same volume, respectively. A variety of crystals of different lengths, thicknesses, and orientations has been observed stemming from the simple evaporation method used. Apparently, thymine crystals grown from the 0.1 mg·ml ^{1} solution have predominantly a rod shape with a diameter of about $2 \pm 1\ \mu$m and a length of 10 100 μm. Increasing solution concentration up to 1.0 mg·ml ^{1} resulted in the presence of microcrystals with flat surfaces (mostly 100 $\times$ 100 μm^2, with RMS roughness <4 nm) and up to 1 5 μm in thickness. These crystals (having different morphologies and fractions of the monohydrate phase) were chosen for the PFM experiments.

After structural and microstructural characterization, PFM experiments have been performed by scanning conducting tip over the surface of thymine microcrystals in a contact mode. Topography (Fig. 2(a)) and both out-of-plane (OOP) and in-plane (IP) PFM signals were acquired (Figs. 2(b) and 2(c)) to get insight into the local piezoelectric properties of thymine. As evidenced by Figs. 2(b) and 2(c), piezoelectric OOP and IP signals have a clear signature of the robust piezoelectricity in thymine. For the OOP component (Fig. 2(b)), the contrast is roughly proportional to the effective d_{33} (longitudinal) coefficient which is determined by the projection of the polarization vector P on the normal N to the crystal surface.[23,42] Since the crystallographic axes were not exactly known, we used common notation for the piezoelectric coefficient where the axis 3 is normal to the major face of the crystal. The observed dark and bright contrasts correspond to the polarization head directed to the thymine crystal surface and to the polarization directed towards the substrate, respectively. This polarization component apparently varies in both sign (polarization direction) and magnitude (amplitude of the effective piezoresponse) depending on the crystallographic orientation of domains or microcrystallites within the polycrystal. According to the

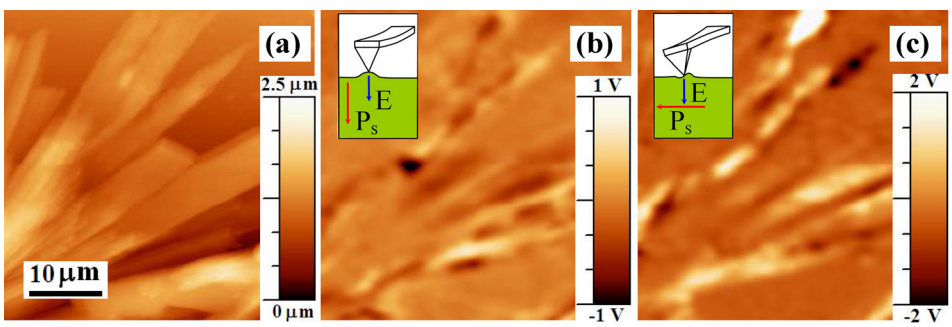

FIG. 2. (a) Topography, (b) OOP PFM, and (c) IP PFM of flat crystals of thymine (1.0 mg ml ^{1} concentration). The inset to (b) and (c) shows schematics of the OOP and IP PFM measurements.

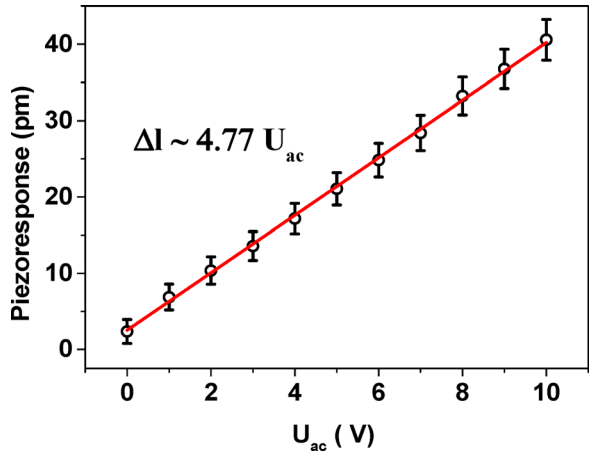

FIG. 3. AC voltage dependence of the OOP displacement.

linearized electrostriction equation, for a ferroelectric material with centrosymmetric paraelectric phase the longitudinal piezoelectric coefficient can be simply expressed as $d_{33} = 2Q\varepsilon_o\varepsilon_{33}P_3$, where Q is the longitudinal electrostriction coefficient, ε_o is the permittivity of vacuum, and ε_3 and P_3 are the dielectric permittivity and spontaneous polarization values, respectively. Therefore, the observed piezoelectric contrast must be related to the variations of spontaneous polarization P (that can be switched by the external electric field if the material is ferroelectric) and dielectric permittivity, ε. The presence of a notable piezoresponse contrast in thymine microcrystals thus proves the existence of spontaneous polarization without any dc bias field in apparent contradiction with early XRD data for pure anhydrate and monohydrate thymine phases.[37,38] Such a behavior (piezoelectricity in a nominally centrosymmetric material) has been previously demonstrated by PFM in $SrTiO_3$ ceramics[43] and at the interfaces.[44]

OOP and IP PFM images (cf. Figs. 2(b) and 2(c)) are complementary, the latter reflecting an effective d_{15} (or d_{24}) shear piezoelectric coefficient, which is proportional to the corresponding in-plane component of the polarization.[45] In general, when the polarization is parallel to the sample surface and perpendicular to the longitudinal axis of the cantilever, the voltage applied to the tip causes an in-plane surface displacement (see inset to Fig. 2(c)). This deformation is then translated via friction into the torsion of the cantilever and is detected by photodetector. A comparison of the topography and PFM images (Fig. 2) attests that the corresponding PFM contrast is independent on the topography, thus providing an evidence of the piezoelectric nature of the signal that often contains an electrostatic (Maxwell force) interaction between the tip and the surface. Apparently, the observed signal does not couple with the topographic features on the crystal surface, e.g., many microcrystals with flat surfaces have a complex domain structure with alternating polarization vectors. This demonstrates that the measured signal is not due to topographic cross-talk, but rather arises from the internal crystal structure (different orientations of polarization vectors in different areas). Another proof is the presence of an IP signal (no electrostatic interaction in this case!) complementary to the OOP contrast. In general, OOP and IP images reflect two different piezoelectric components of piezoresponse signals: vertical $(d_{33})_{\text{eff}}$ and lateral $(d_{15})_{\text{eff}}$.[45] The appearance of such structure unequivocally attests the measured PFM contrast to piezoelectricity as in common piezoelectric materials.[46]

In order to further prove the piezoelectric nature of the signal, we measured the ac voltage dependences of deformation of the sample. The absolute values were obtained by calibrating the surface displacements with the reference sample having similar dielectric properties.[26] Thus obtained value for the longitudinal piezocoefficient for the thymine microcrystal (Fig. 3) is 4.8 pm/V. The absolute value of local piezocoefficient $(d_{33})_{\text{eff}}$ was sufficiently high, varying between 3 and 10 pm/V depending on the location. These values are comparable to those of widely used piezoelectric materials ZnO[47] and AlN[48] and thus can be useful for microelectromechanical applications.

Figure 4(a) demonstrates that the surface of the crystals consists of areas with uniform contrast (polarization domains) separated by domain boundaries. Directions of these boundaries might fit with the intersections of allowed domain walls with the crystal surface.[49] From both topography and PFM images (Figs. 4(a) and 4(b)), we could easily distinguish different contrast colors from the background, corresponding to polarization domains in the investigated thymine crystals. It is well known that ferroelectric domains

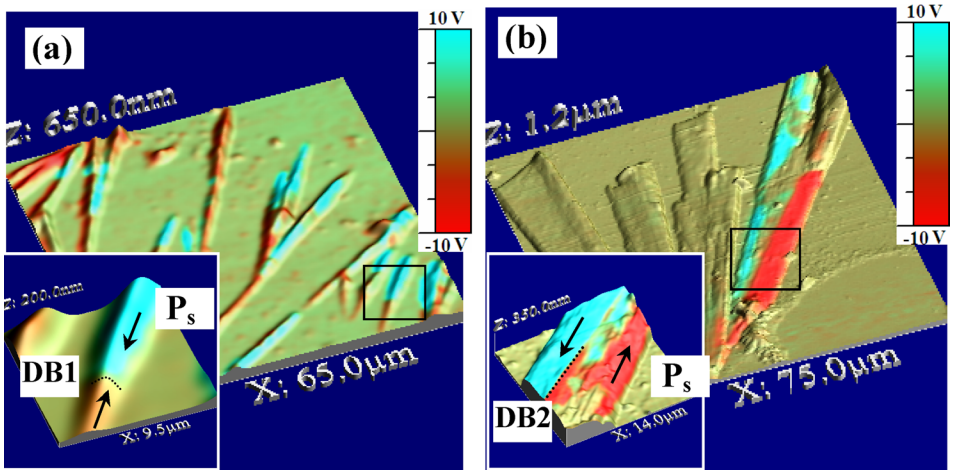

FIG. 4. 3D topography with IP PFM images: (a) needle like crystals (0.1 mg ml ^{1} concentration), (b) flat crystals. (1.0 mg ml ^{1} concentration). DB1 head to head boundary for the domains, DB2 180° domain bound ary. P_s domain polarization.

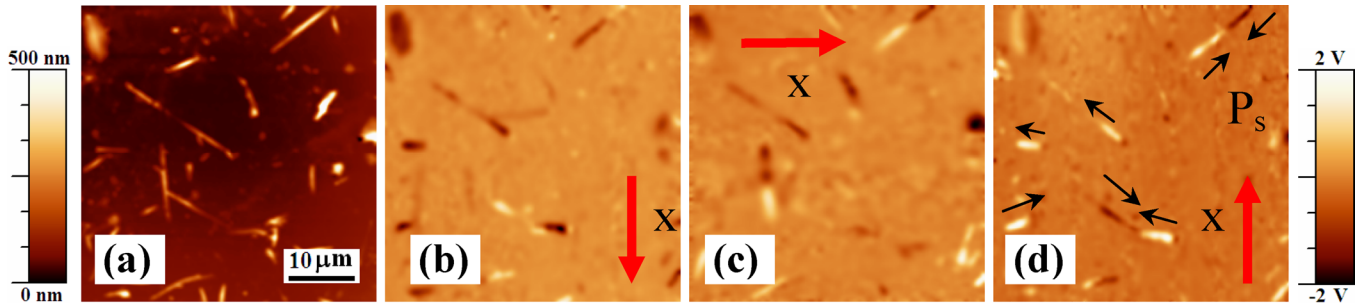

FIG. 5. (a) Topography of thymine microcrystals (0.1 mg ml $^{-1}$ concentration), IP PFM images of thymine before (b) and after rotation at 90° (c) 180° (d). Black arrows show the change in color contrast in domains (red arrows to guide the eye and highlight the sample rotation).

can intersect the surface in well-defined crystallographic orientations, such as 180° domains with the domain boundary along the polar axis.[49] We recorded PFM images of the samples in order to determine the orientation of the domain structures. The images were taken at different positions of the sample. The head-to-head boundary for the domains with polarization parallel to the major crystal axis (DB1, Fig. 4(a)) was clearly observed. The existence of such boundaries involves large polarization discontinuity with the bound charge compensated either by conductivity, or (partly) by zig-zag domain wall geometry.[50] In contrast, a 180° domain boundary (DB2) often appears separating domains with antiparallel polarization directions (Fig. 4(b)).

When the polarization is parallel to the sample surface, the voltage applied to the tip results in an in-plane piezoelectric displacement only. Electrostatic effect (Maxwell stress) is not present and other artifacts (e.g., due to wrong alignment) can be eliminated by the physical rotation of sample. If the sample is rotated by 90° and 180° with the rotation axis normal to the surface, it does not change the topography and vertical signal, however, it changes the IP piezoresponse by reversing its contrast.[26] In order to confirm the piezoelectric nature of the samples, we measured IP contrasts for three different orientations of the sample (Fig. 5). Two different IP images with sample rotation at 90° around the normal to the surface provide two components $(d_{15})_{eff}$ along two orthogonal axis in surface plane (Figures 5(b) and 5(c)). The contrast is completely reversed when the sample is physically rotated at 180° (cf. Figs. 5(b) 5(d)). The observed variation in the IP image is consistent with the piezoelectric nature of thymine crystals.

At higher magnification (Fig. 6), we observed that the micron-sized domains on the surface actually consist of

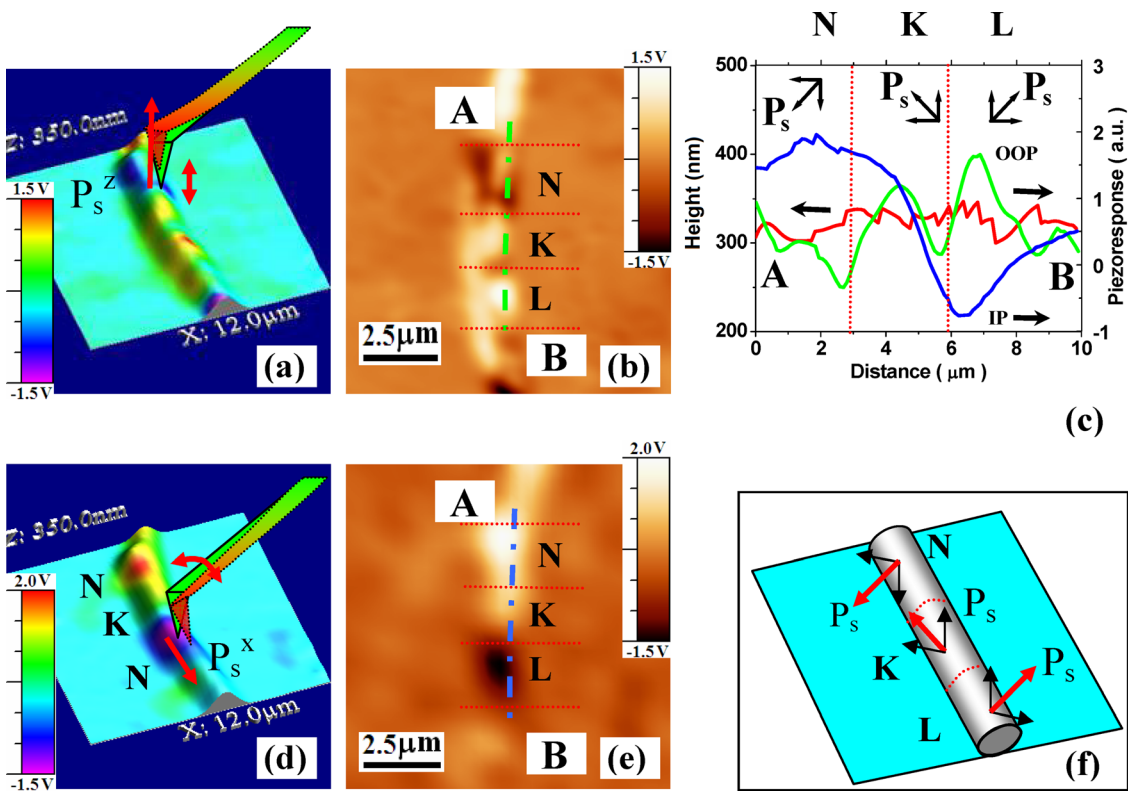

FIG. 6. (a) 3D topography and OOP PFM image, (b) OOP PFM image, (c) cross section topography and PFM images along line AB. (d) 3D topography image with IP PFM data overlaid, (e) IP PFM image, and (f) reconstruction of the polarization direction for three segments along the needle like thymine crystal. (0.1 mg ml $^{-1}$ concentration).

smaller irregular domains with the dimensions down to 1 μm. Generally, for an arbitrary polarization direction, the piezoelectric effect will result in both vertical and torsional displacements, thus allowing for the deconvolution of the static polarization direction, reconstruction of the domain patterns (Fig. 6(c)), and orientation of the molecular structure along the crystal as demonstrated in areas N, K, and L (Fig. 6(f)).

The small size of the thymine molecule and its high dipole moment suggest the possibility of local ferroelectric behavior caused by the so-called "frozen" ordering.[51] The most important characteristic of a ferroelectric is polarization reversal (or switching) by an applied dc electric field. As it is well known, the natural state of a ferroelectric material is a multidomain state.[49] Application of an electric field (poling) will reduce or completely remove domain walls thus achieving a monodomain state. Figure 7 demonstrates the results of local poling in thymine microcrystals. The topography of the scanned area (Fig. 7(a)) was checked both before and after poling, and no changes in topography were detected after the application of dc voltages up to 100 V. In the center of the scanned area, a dc bias of 100 V was applied between the tip and the substrate for 10 s. The piezoresponse contrast was measured in the PFM mode a few minutes after local poling. Figures 7(c) and 7(d) show representative PFM images after poling for both polarities. The contrasts resulting from the application of positive and negative voltages are different in strength (cf. Figs. 7(c) and 7(d)). The induced polarization is unstable and decays with a characteristic relaxation time of the order of 1 hour (Fig. 7(c)). This instability points to the crystal disorder and/or large depolarization field due to incomplete screening (bulk screening) of polarization.[52] To evaluate the switching process of thymine microcrystals, piezoresponse hysteresis loops were acquired locally when the PFM tip was positioned at a selected location and voltage pulses of both polarities were sequentially applied between the tip and Pt bottom electrode (Fig. 8).[27] The loops are characteristic of a local switching process, where the apparent contrast variation is due to the integrated piezoresponse of nascent domain and background (unswitched) polarization.[53,54] The measurements were conducted in the so-called pulse mode. The loop acquisition consists of the application of dc voltage, V_{dc}, for a short time (1 s) while the PFM signal is measured in between the pulses for 1 s with a time constant 300 ms. The voltage was swept by 1 V increments in the ranges $-40\,V < V < +40\,V$, $-60\,V < V < +60\,V$ and $-100\,V < V < +100\,V$. Local poling resulted in a PFM signal consistent with the existence of poled area centered at the poling point. As a result, the observed hysteresis displays a typical ferroelectric-like character and the saturation of the piezoresponse was clearly observed (Fig. 8). The loops reflect local polarization switching under a sufficiently high electric field but were purely dynamic as induced piezoresponse faded away after a few hours. These results are similar to those obtained in ferroelectric relaxors, where the bias-induced reversible ferroelectric-relaxor phase transition resulted in a similar response.[55] This again hints to the significant disorder of the crystals, especially between the layers.

MODELING AND THEORETICAL ANALYSIS

Theoretical analysis of the crystal structure of thymine based on XRD measurements was first performed by Ozeki *et al.*[37] In this work, the authors established a simple two-layer stacking model of individual molecules of thymine anhydrate crystal viewed perpendicular to the plane (001), as well as similar molecular stacking for thymine monohydrate (Figs. 9 and 10). The average interplane spacing between adjacent coplanar layers for monohydrate crystal is 3.4 Å and the molecules are connected by hydrogen bonds and infinite chains, which are superimposed via a simple infinite space translation. The spacing for the anhydrate crystal is 3.36 Å (Ref. 37) (positioned inside the apparent unit cell with space group $P2_1/c$) with the corresponding unit cell parameters a = 12.87 Å, b = 6.83 Å, c = 6.70 Å, $\beta = 105°$ (consistent

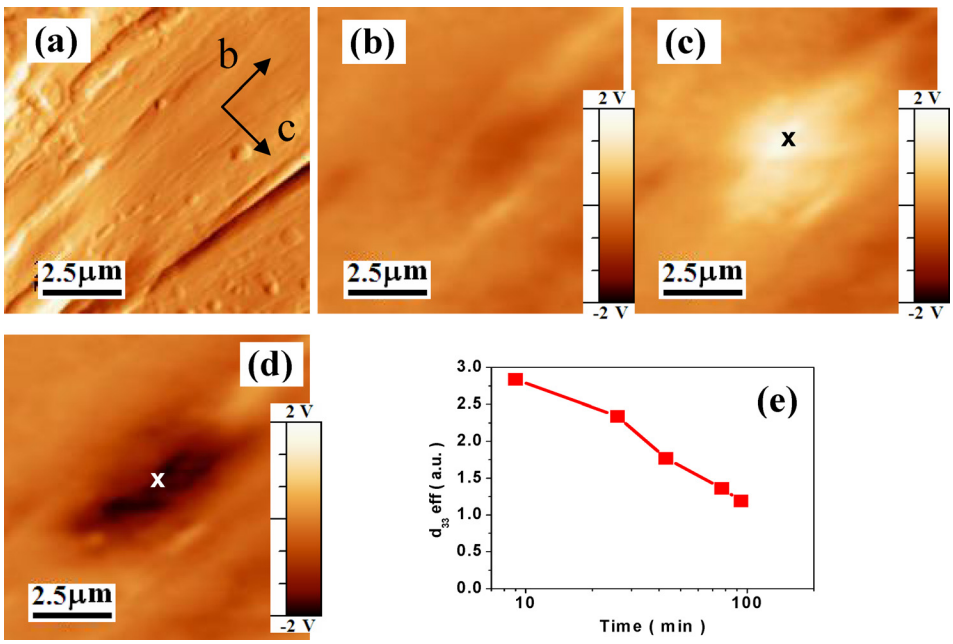

FIG. 7. (a) Topography (deflection) image of a thymine crystal (1.0 mg ml ^{1} concentration). PFM images: (b) before poling, (c) after poling + 100 V for 10 s, (d) after 100 V for 10 s. (x shows the position of poling with the cantilever). (e) Time relaxation of the PFM signal af ter poling + 100 V for 10 s.

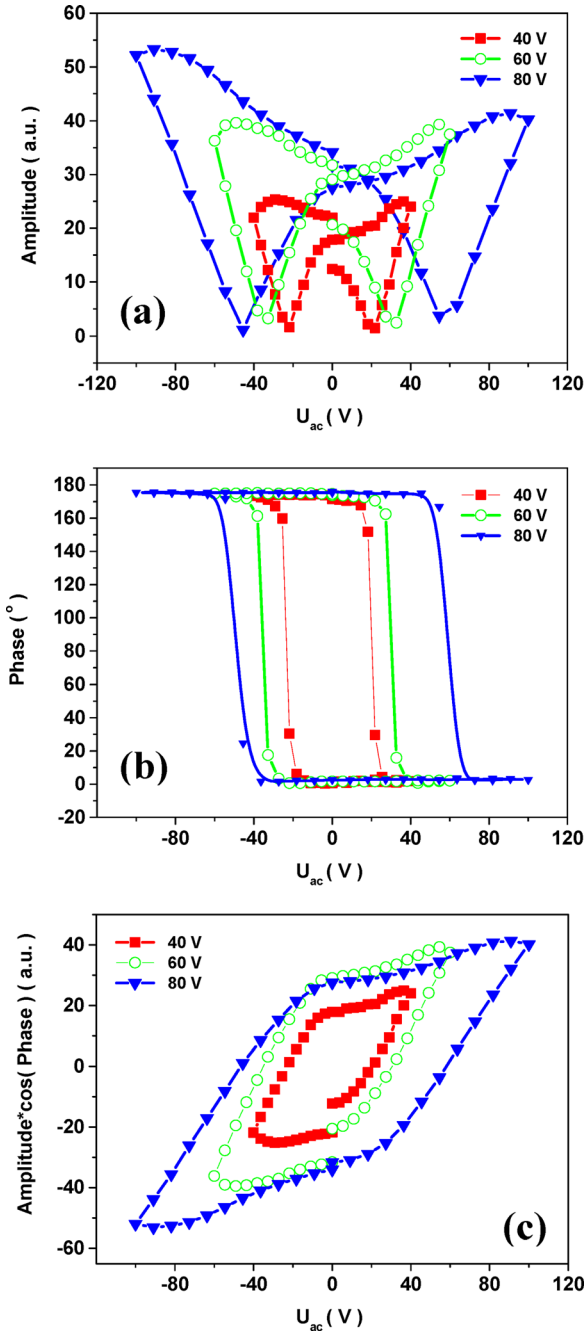

FIG. 8. Piezoresponse hysteresis loops of the thymine microcrystals with different dc voltages (40, 60, and 100 V) recorded with U_{ac} 3 V, 50 kHz. (1.0 mg ml ^{1} concentration). The amplitude $A(\varpi)$ (a), phase difference $\Phi(\varpi)$ (b) and combined piezoresponse $A(\varpi)\cos(\Phi(\varpi))$ (c) of the first harmonic signal of the tip cantilever deflection. The voltage was swept by 1 V increments in the ranges $40\,V < V < +40\,V$, $60\,V < V < +60\,V$ and $100\,V < V < +100\,V$.

with our XRD data). There are totally 4 molecules in the unit cell. Further, the hydrogen bonds distances were analyzed and found to be different for monohydrate and anhydrate crystals. In earlier publications (Refs. 37 and 38), the positions of *all* existing hydrogen atoms were not taken into account. Only 9 main atoms for each thymine molecule were considered in these calculations.

Here, we constructed a full molecular model of a thymine molecule consisting of additional 6 hydrogen atoms (15 atoms in total), forming a hydrogen bond network, and,

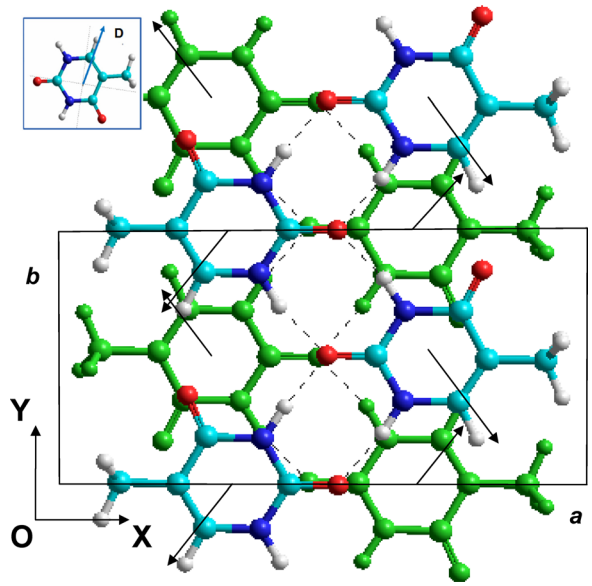

FIG. 9. Molecular model of two layered thymine structure in XOY plane. Straight lines show the unit cell with lattice parameters ***a*** and ***b***. Dashed lines shown hydrogen bonds. Arrows show the orientation of the individual dipole of thymine molecules. Second (or down) layer is marked by green colour. Distance between layers in OZ direction (along c axis) is approximately ~3.4 Å. Colours of atoms: Oxygen red, Nitrogen blue, Carbon cyan, Hydrogen grey. Inset shows the individual dipole of one thymine molecule, **D** ~ 4.5 Debye (computed PM3 UHF).

based on it, a full unit cell comprising all 60 atoms. Then, using available experimental crystallographic data, we applied local density approximation (LDA) of density functional theory (DFT) with first-principle calculations on the base of AIMPRO code[32,56] to obtain optimized crystallographic structures containing all atomic positions. This is important because XRD measurements cannot determine H positions or C-H bond lengths. It is also essential that the chosen unit cell contains only 2 full thymine molecules and parts of 2 adjacent molecules (shown as rectangles in Fig. 9), which are continued in the adjacent unit cell following infinite translation.

These calculations allowed us to construct a viable two-layer model of a thymine crystal structure. In two-layer

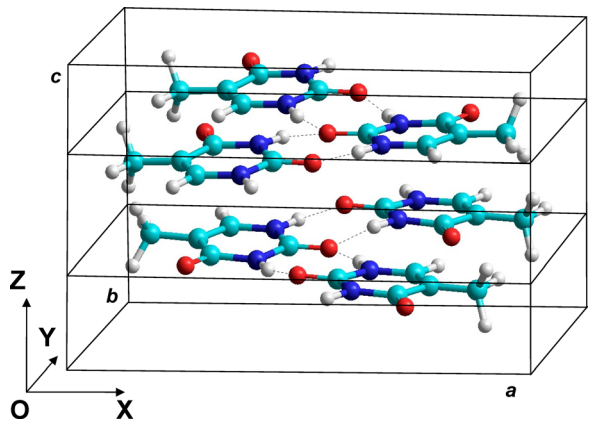

FIG. 10. 3D image of the molecular structure of the thymine crystal, represent the two layered location of the individual thymine molecules in one unit cell with lattice parameters ***a, b, c.*** This model constructed using HyperChem 8.01 options.

TABLE I. HyperChem PM3 UHF data for isolated nucleotide of DN base pair.

Base	Dipole moment, Debye
Adenine	2.495
Cytosine	6.074
Guanine	5.45
Thymine	4.51

model, each layer is the same as in one-layer model, but both have opposite directions of dipole moments (for each thymine molecule and for the entire layer) between the first and second layers. Planar images are shown in Fig. 9 and 3D images (with labelled unit cell) are reproduced in Fig. 10. This model is in a full agreement with the earlier reported data.[33,37] However, taking into account hydrogen atoms and their effect on the final structure, we could calculate the lengths of hydrogen bonds and dipole moments of the individual thymine molecules (D ≈ 4.5 Debye, see Table I) for the entire crystal structure. We could determine the polarization of thymine (as well as other physical parameters) in various volume partitions and directions. As a result, the dipole moments in two-layer model compensate each other and their sum equals zero (which is indeed centrosymmetric). Non-zero polarization must exist at *small* dimensions (presumably at the surface) where it is not compensated, being also switchable as it will be shown below. It should be noted that the PFM method is collecting piezoresponse from the surface of the crystal and thus the presented two-layer model can be still viable and used to roughly describe the experimental results obtained in this work. Recent theoretical calculations of flexural piezoelectric coupling can be also used to describe piezoelectricity in 2D materials with centrosymmetric structure.[57,58]

In order to estimate the polarization value, we constructed the minimal molecular cluster consisting of four thymine molecules in one layer, which describe the minimal symmetrically compensated molecular cluster unit within coplanar layers. Based on it, we then considered a two-layer molecular model of eight thymine molecules with oppositely oriented dipole moments. However, all essential features of polarization switching could be obtained based on one-layer model. For these calculations we used HyperChem 8.0 tools as described previously in a number of papers.[27,34–36,59] Using this approach, we developed a simple molecular model for

TABLE II. The physical parameters (calculated and experimental ones) cal culated for different directions of the applied electric field ΔE_i ±0.001 a.u. 5.1422 MV/cm for i X, Y, Z. Note that the induced polarization and piezocoefficient is symmetric for X and Z axes, and asymmetric for the field applied along Y axis (i.e., Y_+, Y directions).

Axis	P_i, $\mu C/cm^2$	ΔP_i, $\mu C/cm^2$	ε_i	Q_i, m^4/C^2	d_i	$2\varepsilon_i\varepsilon_o Q\,\Delta P_i$, pm/V	$d_{i,exp.}$, pm/V
X	0	1.2	5.6	8.5		10.1	∼10
Y	11.410	Y_+ 0.58	4	25		10.6	∼10
		Y 1.2	4	5		4.3	
Z	0	0.8	1.4	8.5		2	…

thymine molecular unit based on the reported unit cell of the crystal (consisting of four thymine molecules lying in one plane, Fig. 11). In this model, we established that the main polarization direction lies along OY axis with spontaneous polarization $P = P_y \approx 11.4\,\mu C/cm^2$ (see Fig. 11(a) and Table II). Further, we simulated the application of an external electric field along this axis ($E_{yc} \approx 0.0175$ a.u. ≈ 90 MV/cm) and found that P_y can be decreased to zero under this electric field but the polarization cannot be switched. For the two-layer model with oppositely oriented dipoles along OY axis, the total dipole moment and, consequently, the polarization is fully compensated for stacking molecules in adjacent layers. The resulting total moment is zero and there is no polarization in this centrosymmetric structure. However, in both cases, it is possible to switch the direction of the polarization in the perpendicular direction, OX, thereby changing the sign of the piezoresponse (see Fig. 11(b) and Table II). The simulation of polarization switching gives the difference between the two polarization states $\Delta P_x \approx 8.27\,\mu C/cm^2$ (under electric field along OX $\Delta E_x \approx \pm$ 0.01 a.u. ≈ 51.422 MV/cm). If lower field is applied ($\Delta E_x \approx \pm$ 0.001 a.u. ≈ 5.1422 MV/cm) the switching polarization is much lower $\Delta P_x \sim 1.2\,\mu C/cm^2$ but still should be experimentally measurable. In the OZ direction, the polarization $P_z \approx 0$ reflecting centrosymmetric structure, which forms a coplanar configuration in the XOY plane.[60–63] The switching polarization, ΔP_z, is much lower in this case (see Table II for details) and does not correspond to the experimental situation.

The analysis of the hydrogen bond network yields the following lengths of the hydrogen bonds in our system: 2.78… 2.82 Å for N O atoms, 0.995… 1.0175 Å for N H atoms, and 1.68…1.84 Å for C H bonding. The bond length between C and O atoms is more stable, being in the range

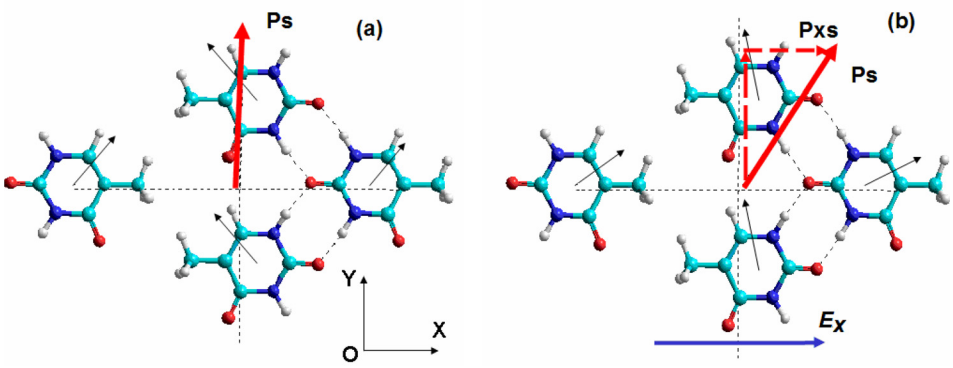

FIG. 11. Model of thymine under an electric field (ab plane). (a) Without electric field and (b) under electric field along OX.

1.225 1.228 Å. It is important that the calculated data are consistent with earlier reports[37,38] but represent more accurate calculations. One of the salient features obtained in the model is that the neighboring individual thymine molecules in the same plane are inclined relative to each other at the angle of about 5 6°, being very close to the results obtained in Ref. 37. These results are in line with another model taking into account the interactions between two coplanar base pairs,[62] where a mandatory tilt angle was shown to exist between the two nucleobases in DNA structures. This additionally confirms the validity of our calculations.

Further, using molecular simulations based on the simple thymine model we could calculate the corresponding polarizability and dielectric constant of thymine $\varepsilon \sim 4$ 5.6 and longitudinal piezoelectric coefficient $d_{xx/yy} \sim 10.8$ pC/N in the OX and OY directions for the applied electric field ~ 5.14 MV/cm, respectively. The latter value is in a good agreement with the experimental data obtained by PFM and is comparable with those of other organic and biological molecular structures.[64–67] As it is clear from the introduced model, the d_{zz} coefficient has a very strong asymmetry for the field applied along OY axis, as shown in Table II.

The significance of thymine monohydrate phase present in our microcrystals is not clear at the moment and future work is underway to understand the role of water molecules and details of structural changes leading to an apparent loss of the inversion center in thymine microcrystals. Ferroelectric-like behavior could result from both bulk effects (as in relaxor ferroelectrics where disorder destroys the long-range ferroelectric orderg) or due to interfaces.[44] Ferroelectric-like behavior is a direct consequence of a large dipole moment of molecular thymine and adds a new functionality to this important biomaterial. Further studies of the observed electromechanical coupling and possible ferroelectricity in thymine and other nucleobases are indispensable to understand the role of hydrogen bonding in the observed polar behavior.

CONCLUSIONS

Experimental results and complementary computer modeling point to the presence of local piezoelectric and ferroelectric properties in thymine microcrystals grown from the solution The obtained values of polarization and piezoelectric coefficients are high enough (several times greater than in quartz!) and can be used in various micromechanical applications. These results provide a pathway for developing new organic piezoelectric materials based on DNA nucleobases and open up the potential of thymine for applications based on the observed piezoelectric and polar properties.

ACKNOWLEDGMENTS

This research was partially supported by the European Commission within FP7 Marie Curie Initial Training Network "Nanomotion" (Grant Agreement No. 290158). I. Bdikin would like to thank the Ciência 2008 Program (FCT). V. Bystrov is thankful to FCT for partial financial support within his Grant No. SFRH/BPD/22230/2005 and with RFBR Grant No. 15-01-04924. The authors are also grateful to FCT (Project No. REDE/1509/RME/2005) for the equipment use and scientific and technical assistance. The authors are thankful to Jose Coutinho for the opportunity and helpful assistance in the calculations in AIMPRO code on the Blafis cluster at the Physical Department of the University of Aveiro. This work was developed in the scope of the project CICECO-Aveiro Institute of Materials (Ref. FCT UID/CTM/50011/2013), financed by national funds through the FCT/MEC and when applicable co-financed FEDER under the PT2020 Partnership Agreement.

[1]R. P. Sinha and D. P. Hader, Photochem. Photobiol. Sci. **1**, 225 (2002).
[2]J. D. Watson and F. H. C. Crick, Nature **171**, 737 (1953).
[3]F. H. C. Crick, in *Symp. Soc. Exp. Biol. XII* (Cambrige University Press, 1958), pp.139 163.
[4]P. W. K. Rothemund, Nature **440**, 297 (2006).
[5]K. Hansma, B. Drake, O. Marti, S. A. C. Gould, and C. B. Prater, Science **243**, 641 (1989).
[6]C. Leung, A. Bestembayeva, R. Thorogate, J. Stinson, A. Pyne, Ch. Marcovich, J. Yang, U. Drechsler, M. Despont, T. Jankowski, M. Tschope, and B. W. Hoogenboom, Nano Lett. **12**, 3846 (2012).
[7]T. Boland and B. D. Ratner, Proc. Natl. Acad. Sci. U. S. A. **92**, 5297 (1995).
[8]V. D. Lakhno, Int. J. Quantum Chem. **108**, 1970 (2008).
[9]C. Dekker and M. A. Ratner, Phys. World **14**, 29 (2001).
[10]J. D. Slinker, N. B. Muren, S. E. Renfrew, and J. K. Barton, Nat. Chem. **3**, 228 (2011).
[11]C. J. Murphy, M. R. Arkin, Y. Jenkins, N. D. Ghatlia, S. H. Bossmann, N. J. Turro, and J. K. Barton, Science **262**, 1025 (1993).
[12]H. W. Fink and C. Schonenberger, Nature **398**, 407 (1999).
[13]S. O. Kelley and J. K. Barton, Science **283**, 375 (1999).
[14]L. V. Yakushevich, Phys. Lett. A. **136**, 413 (1989).
[15]Th. B. Singh, N. S. Sariciftci, and J. G. Grote, Adv. Polym. Sci. **223**, 73 (2010).
[16]M. Jakobsson and S. Stafstrom, J. Chem. Phys. **129**, 125102 (2008).
[17]Y. A. Berlin, A. L. Burin, and M. A. Ratner, J. Am. Chem. Soc. **123**, 260 (2001).
[18]E. Louis, F. Yndurain, and F. Flores, Phys. Rev. B **13**, 4408 (1976).
[19]C. Tejedor and F. Flores, J. Phys. C **11**, L19 (1978).
[20]M. Y. Choi and R. E. Miller, J. Phys. Chem. A **111**, 2475 (2007).
[21]S. Tombelli, M. Minunni, A. Santucci, M. M. Spiriti, and M. Mascini, Talanta **68**, 806 (2006).
[22]D. Ehrlich, L. Carey, J. Chiou, S. Desmarais, S. El Difrawy, L. Koutny, R. Lam, P. Matsudaira, B. Mckenna, L. Mitnik Gankin, T. O'Neil, M. Novotny, A. Srivastava, P. Streechon, and W. Timp, Proc. IEEE Sens. **1**, 448 (2002).
[23]M. P. Nikiforov, G. L. Thompson, V. V. Reukov, S. Jesse, S. Guo, B. J. Rodriguez, K. Seal, A. A. Vertegel, and S. V. Kalinin, ACS Nano **4**, 689 (2010).
[24]A. Gruverman, D. Wu, B. J. Rodriguez, S. V. Kalinin, and S. Habelitz, Biochem. Biophys. Res. Commun. **352**, 142 (2007).
[25]B. J. Rodriguez, S. V. Kalinin, J. Shin, S. Jesse, V. Grichko, T. Thundat, A. P. Baddorf, and A. Gruverman, J. Struct. Biol. **153**, 151 (2006).
[26]A. Kholkin, N. Amdursky, I. Bdikin, E. Gazit, and G. Rosenman, ACS Nano **4**, 610 (2010).
[27]A. Heredia, V. Meunier, I. K. Bdikin, J. Gracio, N. Balke, S. Jesse, A. Tselev, P. K. Agarwal, B. G. Sumpter, S. V. Kalinin, and A. L. Kholkin, Adv. Funct. Mater. **22**, 2996 (2012).
[28]S. B. Lang, S. A. M. Tofail, A. L. Kholkin, M. Wojtas, M. Gregor, A. A. Gandhi, Y. Wang, S. Bauer, M. Krause, and A. Plecenik, Sci. Rep. **3**, 2215 (2013).
[29]H. Zheng, Q. Zhan, F. Zavaliche, M. Sherburne, F. Strau, M. P. Cruz, L. Q. Chen, U. Dahmen, and R. Ramesh, Nano Lett. **6**, 1401 (2006).
[30]N. Balke, I. Bdikin, S. V. Kalinin, and A. L. Kholkin, J. Am. Ceram. Soc. **92**, 1629 (2009).
[31]N. A. Pertsev, A. Petraru, H. Kohlstedt, R. Waser, I. K. Bdikin, D. Kiselev, and A. L. Kholkin, Nanotechnology **19**, 375703 (2008).
[32]See http://aimpro.ncl.ac.uk/ for AIMPRO | AIMPRO. abinitio Official Site.
[33]G. Portalone, L. Bencivenni, M. Colapietro, A. Pieretti, R. F. amondo, J. Møller, A. Senning, X. K. Yao, H. G. Wang, J. P. Tuchagues, and M. Ogren, Acta Chem. Scand. **53**, 57 (1999).

[34]V. S. Bystrov, E. V. Paramonova, I. K. Bdikin, A. V. Bystrova, R. C. Pullar, and A. L. Kholkin, J. Mol. Mod. **19**, 3591 (2013).
[35]See http://www.hyper.com/?tabid 360 for HyperChem (2002), Tools for Molecular Modeling (release 7, 8), Professional edition, Gainesville: Hypercube, Inc. Home Page (accessed May 12, 2014).
[36]V. S. Bystrov, E. Paramonova, I. Bdikin, S. Kopyl, A. Heredia, R. Pullar, and A. Kholkin, Ferroelectrics **440**, 3 (2012).
[37]K. Ozeki, N. Sakabe, and J. Tanaka, Acta Crystallogr., Sect. B: Struct. Crystallogr. Cryst. Chem. **25**, 1038 (1969).
[38]R. Gerdil, Acta Cryst. **14**, 333 (1961).
[39]S. Goshen, D. Mukamel, and H. Shaked, Phys. Rev. B **2**, 4679 (1970).
[40]A. L. Kholkin, E. K. Akdogan, A. Safari, P. F. Chauvy, and N. Setter, J. Appl. Phys. **89**, 8066 (2001).
[41]Sh. Dai, M. Gharbi, P. Sharma, and H. S. Park, J. Appl. Phys. **110**, 104305 (2011).
[42]S. V. Kalinin, B. J. Rodriguez, S. Jesse, T. Thundat, and A. Gruverman, Appl. Phys. Lett. **87**, 053901 (2005).
[43]A. L. Kholkin, I. K. Bdikin, T. Ostapchuk, and J. Petzelt, Appl. Phys. Lett. **93**, 222905 (2008).
[44]C. W. Bark, P. Sharma, Y. Wang, S. H. Baek, S. Lee, S. Ryu, C. M. Folkman, P T. R. Audel, A. Kumar, S. V. Kalinin, A. Sokolov, E. Y. Tsymbal, M. S. Rzchowski, A. Gruverman, and C. B. Eom, Nano Lett. **12**, 1765 (2012).
[45]L. M. Eng, M. Abplanalp, and P. Guner, Appl. Phys. A: Mater. Sci. Process. **66**, S679 (1998).
[46]S. V. Kalinin, A. N. Morozovska, L. Q. Chen, and B. J. Rodriguez, Rep. Prog. Phys. **73**(5), 056502 (2010).
[47]I. K. Bdikin, J. Gracio, R. Ayouchi, R. Schwarz, and A. L. Kholkin, Nanotechnology **21**, 235703 (2010).
[48]M. A. Dubois and P. Mural, Appl. Phys. Lett. **74**, 3032 (1999).
[49]B. A. Strukov and A. P. Levanyuk, *Ferroelectric Phenomena in Crystals: Physical Foundations* (Springer, London, 2011).
[50]A. A. Tagantsev, L. E. Cross, and J. Fousek, *Domains in Ferroic Crystals and Thin Films* (Springer, New York, 2010).
[51]Zh. Sun, X. Wang, J. Luo, Sh. Zhang, D. Yuan, and M. Hong, J. Mater. Chem. C **1**, 2561 (2013).
[52]V. Ya. Shur and E. L. Rumyantsev, Ferroelectrics **191**, 319 (1997).
[53]S. V. Kalinin, A. Gruverman, and D. A. Bonnell, Appl. Phys. Lett. **85**, 795 (2004).
[54]A. Wu, P. M. Vilarinho, V. V. Shvartsman, G. Suchaneck, and A. L. Kholkin, Nanotechnology **16**, 2587 (2005).
[55]V. V. Shvartsman, A. L. Kholkin, M. Tyunina, and J. Levoska, Appl. Phys. Lett. **86**, 222907 (2005).
[56]P. R. Briddon and M. J. Rayson, Phys. Status Solidi B **248**, 1309 (2011).
[57]K. A. N. Duerloo, M. T. Ong, and E. J. Reed, J. Phys. Chem. Lett. **3**, 2871 (2012).
[58]K. A. N. Duerloo and E. J. Reed, Nano Lett. **13**, 1681 (2013).
[59]P. R. Briddon and R. Jones, Phys. Status Solidi B **217**, 131 (2000).
[60]L. Lehninger, *Biochemistry: The Molecular Basis of Cell Structure and Function* (Worth Pub, Inc., New York, 1972).
[61]A. V. Kabanov and V. M. Komarov, Int. J. Quantum Chem. **88**, 579 (2002).
[62]J. Musil, O. Novakova, and K. Kunz, *Biochemistry in Schematic Perspective* (Avicenum, Czechoslovak Medical Press, Prague, 1984).
[63]P. Yakovchuk, E. Protozanova, and M. D. Frank Kamenetskii, Nucl. Acids Res. **34**, 564 (2006).
[64]J. J. Dwyer, A. G. Gittis, D. A. Karp, E. E. Lattman, D. S. Spencer, W. E. Stites, and E. B. García Moreno, Biophys. J. **79**, 1610 (2000).
[65]C. Halperin, S. Mutchnik, A. Argronin, M. Molotskii, P. Urenski, M. Salai, and G. Rosenman, Nano Lett. **4**, 1253 (2004).
[66]J. R. C. Maarel, Biophys. J. **76**, 2673 (1999).
[67]C. H. Kim, C. Jung, H. G. Park, and Y. K. Choi, BioChip J. **2**, 127 (2008).